Available online at www.sciencedirect.com

SciVerse ScienceDirect

Ceramics International 39 (2013) 8183–8188

CERAMICS INTERNATIONAL

www.elsevier.com/locate/ceramint

A hydrothermal synthesis of eggshell and fruit waste extract to produce nanosized hydroxyapatite

Shih-Ching Wu[a,b], Hsi-Kai Tsou[c], Hsueh-Chuan Hsu[a,b], Shih-Kuang Hsu[a,b], Shu-Ping Liou[d], Wen-Fu Ho[e,*]

[a]Department of Dental Technology and Materials Science, Central Taiwan University of Science and Technology, Taiwan, ROC
[b]Institute of Biomedical Engineering and Materials Science, Central Taiwan University of Science and Technology, Taiwan, ROC
[c]Department of Neurosurgery, Taichung Veterans General Hospital, Taichung, Taiwan, ROC
[d]Department of Mechanical and Automation Engineering, Da-Yeh University, Taiwan, ROC
[e]Advanced Materials and BioMaterials Lab, Department of Materials Science and Engineering, Da-Yeh University, Taiwan, ROC

Received 20 March 2013; received in revised form 29 March 2013; accepted 30 March 2013
Available online 9 April 2013

Abstract

Eggshells are typically considered to be garbage because they have no value as food but they favor microbial growth. Vast quantities of eggshell waste are available from food processing, baking, and hatching industries. The present study provides a simple hydrothermal method to obtain high-purity hydroxyapatite (HA) nanoparticles from eggshells and three kinds of fruit waste extracts: grape, sweet potato, and pomelo peels. These synthesized nanoparticles have been characterized by X-ray diffraction, Fourier transform infrared spectroscopy, and scanning electron microscopy studies. The results showed that hydrothermal reaction times and biomolecule amounts influenced product shape, product size, and synthetic HA crystal morphology. The HA taken from pomelo peelings exhibited good aspect ratios with physical shapes similar to those of the crystalline HA structures of natural human bone. HA synthesized from eggshell powders contains several important trace elements, such as Na, Mg, and Sr.

Keywords: Eggshell; Hydroxyapatite; Nanoparticles; Waste materials; Hydrothermal

1. Introduction

Hydroxyapatite (HA) has been widely used as an implant material due to its close similarity in composition to natural bone. Many studies have shown that HA ceramics show no toxicity, no inflammatory response, no pyrogenetic response, no fibrous tissue formation between implant and bone, and the ability to bond directly to the host bone [1–3]. Artificial HA has many applications, such as bone graft substitutes, sustained-release drug delivery devices, and protein purification [4,5].

However, the mineral composition of human bone differs slightly from stoichiometric HA due to the impurities in human bone, which include carbonate, chloride, fluoride, magnesium, and sodium [6,7]. The natural apatite of the human body contains approximately 3–8 wt% of carbonate [8]. Natural bone tissue includes tiny HA crystals in its nano-regime [9]. Nanosized HA exhibits much higher bioactivity than coarser crystals; nanophase ceramics made from nanosized HA may help osteoblasts to synthesize alkaline phosphatase. Such ceramics may also promote the adhesion and proliferation of cells and lead to rapid repair of hard tissue injuries [10].

Over the past several years, biologically derived natural materials such as bovine bones [11], fish bones [12], oyster shells [13], corals [14–16] and eggshells [17] have been converted into useful biomaterials like HA. Biological HA obtained from natural resources preserves some properties of the precursor material, such as pore structure and chemical composition [18]. In 1974, Roy and Linnehan [14] simplified the field by taking a biomimetic approach that employed the direct conversion of coral calcium carbonate skeletons into HA

*Correspondence to: Department of Materials Science and Engineering, Da-Yeh University, 168 University Road, Dacun, Changhua, Taiwan 51591, ROC. Tel.: +886 4 851 1888x4108; fax: +886 4 851 1280.
E-mail addresses: fujii@mail.dyu.edu.tw, titi0918@yahoo.com.tw (W.-F. Ho).

0272-8842/$ - see front matter © 2013 Elsevier Ltd and Techna Group S.r.l. All rights reserved.
http://dx.doi.org/10.1016/j.ceramint.2013.03.094

(termed coralline HA). Sivakumar et al. [15] used a hydrothermal process to derive HA from corals from the Gulf of Mannar, off the coast of India. Hydrothermal conversion of Australian corals into HA was studied by Hu et al. [16]. However, some coral species are in danger of extinction and most coral species have slow growth rates. Therefore, it is urgent to explore new alternative materials that are renewable, low-priced, and easily accessible.

Avian eggshell has a mineral composition similar to corals. Eggshells have been introduced as a candidate material for maxillofacial and craniofacial surgery because avian eggshells can be procured easily [19,20]. Fresh eggshell typically consists of a three-layered structure; the cuticle on the outer surface resembles a ceramic; the middle layer is spongy; the inner layer consists of lamellar layers. The eggshell represents approximately 11% of the total weight of egg. The chemical composition (by weight) of chicken eggshell consists of calcium carbonate (94%), magnesium carbonate (1%), calcium phosphate (1%), and organic matter (4%) [21]. Chicken eggshells contain trace elements, such as Na, Mg, and Sr, which are also found in human bone. Chicken eggshells that would normally be discarded as garbage can be used as high-quality calcium sources for the preparation of HA; this incidentally eliminates the cost of recycling or garbage disposal [21].

A number of synthetic routes have been developed for preparing HA powders, such as mechanochemical, sol–gel, chemical precipitation, hydrothermal, and microemulsion methods. Among the various synthetic routes, the hydrothermal method has been proven to be an effective and convenient process to prepare HA batches with diverse controllable morphologies and architectures [22]. In addition, there is an ever-growing need to develop clean, non-toxic, and environmentally friendly procedures for nanoparticle synthesis. In the present investigation, eggshell and several biomolecules from waste materials (pomelo, grape, and sweet potato peel extracts) have been used for the synthesis of nanosized HA through a hydrothermal method.

2. Materials and methods

Biowaste eggshells were cleaned and crushed into powder. Then, 2 g of that powder was dissolved in 20 ml 1:3 hydrochloric acid/water solution. Three solutions were prepared from three different kinds of fruit waste. Each solution used 80 g by weight of fruit waste and 1000 ml of water. The fruit wastes were grape, sweet potato, and pomelo peels. The polyphenolic compounds and beta-carotene are found in the grape peel extract [23]. The sweet potato peel extract contains several phytochemicals such as polyphenols and carotenoids [24]. The main ingredients of pomelo peel extract are flavonoids, dietary fibers and essential oils [25]. The pomelo peel oils consist mainly of limonene [26]. Each 80 g waste sample was boiled in 1000 ml of water for 10 min and then filtered. Five millilitre of this filtrate was added to 20 ml of the above eggshell solution and stirred gently but thoroughly. 0.85 ml (i.e. Ca/P molar ratio = 1.67) of 85% phosphoric acid was added little by little to the stirred mixture. NH_4OH solution was added to keep the solution pH at 10. The mixtures were sealed in polytetrafluoroethylene (Teflon)-lined stainless steel autoclaves and hydrothermal transformations took place at 150 °C for different reaction times (24 and 72 h) in independent experiments. The autoclaves were allowed to cool to room temperature naturally. The resulting products were powders; they were collected, rinsed with deionized water, and dried at 60 °C for 24 h, prior to examination.

The crystalline phases of the synthesized powders were analyzed by powder X-ray diffraction with CuKα radiation (XRD; XRD-6000, Shimadzu, Japan). The phases were identified by comparing the experimental X-ray diffractograms to standards compiled by the Joint Committee on Powder Diffraction Standards (JCPDS). Microstructural observation was conducted using a scanning electron microscope (SEM; JSM-6700 F, JEOL, Japan) under secondary electron mode. Surface chemical analysis was performed using energy-dispersive X-ray spectroscopy (EDS) coupled with the SEM. Fourier transform infrared (FT-IR; Bio-Rad, FTS-40, USA) spectra were obtained in the region 550–4000 cm^{-1} from the powdered samples. In order to evaluate the composition of the synthesized powders and the presence of heavy metals, inductively coupled plasma-atomic emission spectrometry (ICP-AES; ICAP 9000, Jarrell-Ash Co., USA) analysis was performed.

3. Results and discussion

3.1. X-ray diffraction analysis

To get homogeneous nanopowder, a template for regulating particle growth is required [27]. In this research, three kinds of biomolecular templates from waste materials were used to investigate influences on the crystallization, morphology and size of nano-HA particles. Fig. 1 shows the X-ray diffraction patterns of the synthesized nano-HA batches in the presence of the three different biomolecules. As shown in this figure, HA samples synthesized using three different biomolecules had similar XRD patterns and no other crystalline phase was observed besides HA. All the diffraction peaks were assigned to monophase low-crystalline HA. This indicates that the use of varied biomolecules had not hindered the formation of HA phases. The six broad peaks of the XRD patterns indicate that the HA particles had small sizes and low crystallinity; these characteristics resemble those of naturally occurring bone apatite. The low-crystalline apatite structures obtained in this study should be expected to be more metabolically active than fully-developed crystalline HA structures. Such fully-developed crystals have low biodegradability in physiological environments [28].

Here, the XRD patterns of only one prepared sample for each condition are presented, because all the cases were similar. Fig. 1 compares three curves for 24 h reactions to the corresponding curves for 72 h reactions; the 72 h curves had narrower, more distinct HA peaks; this suggests an

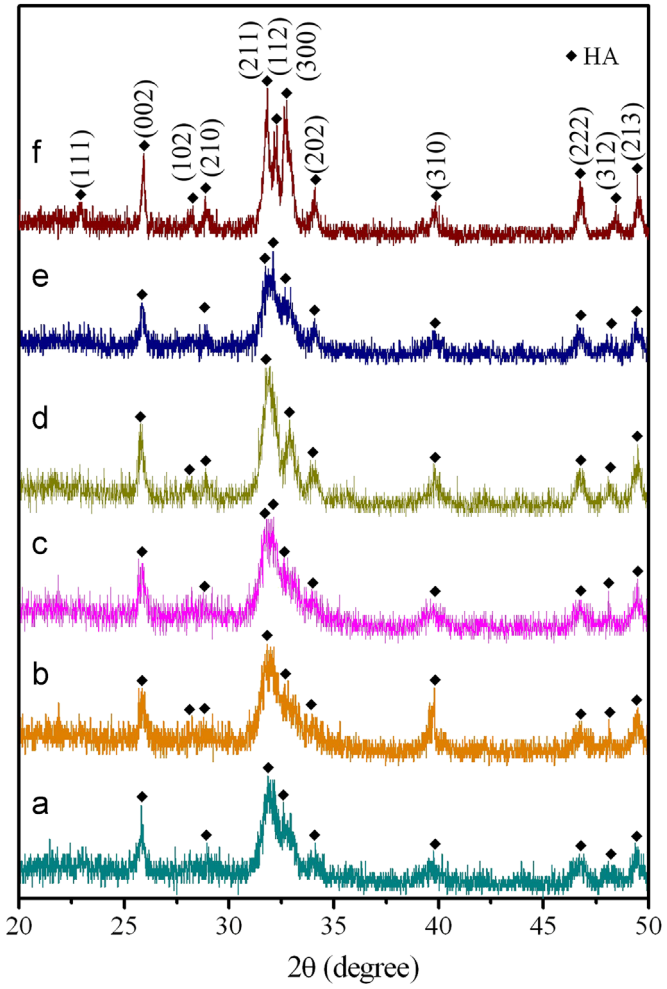

Fig. 1. XRD patterns of hydroxyapatite synthesized using three kinds of biomolecular templates in waste by hydrothermal treatment at 150 °C for 24 or 72 h. (a) Grape peel, 24 h; (b) grape peel, 72 h; (c) sweet potato peel, 24 h; (d) sweet potato peel, 72 h; (e) pomelo peel, 24 h and (f) pomelo peel, 72 h.

increase in crystallinity. It is more significant for the pattern of HA synthesized using the extraction of pomelo peel.

3.2. Fourier transform infrared analysis

Fig. 2 presents FT-IR spectra of HA nanopowders synthesized in the presence of biomolecular templates after hydrothermal reactions at 150 °C for 72 h. FT-IR tested for the presence of functional groups like phosphate and carbonate. Note that, all HA synthesized with three different biomolecular templates have similar FT-IR spectra. In the spectra, bending and stretching modes of P–O vibrations are present as bands around 554 and 1031 cm^{-1}, respectively. The bands at 2851 and 2920 cm^{-1} are attributed to the asymmetric stretching of CH_2 and CH_3 [29]. Besides these spectra, bands at 631 and 3580 cm^{-1} represent structural OH groups. Additionally, the carbonate ion substitution is identified by characteristic peaks of the carbonate ions around 864 and 1434 cm^{-1}, which are attributed to the vibrational modes of the carbonate ions substituted at the phosphate sites (B-type) [30]. Moreover,

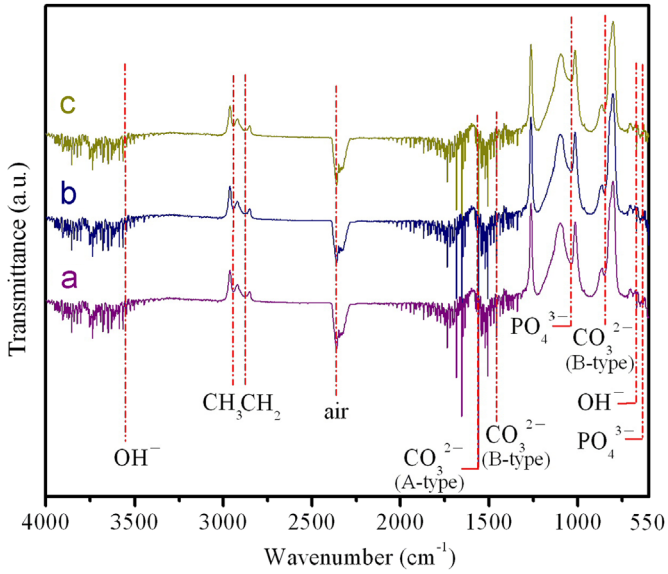

Fig. 2. FT-IR spectra of hydroxyapatite synthesized using three kinds of biomolecular templates in waste by hydrothermal treatment at 150 °C for 72 h. (a) Grape peel, (b) sweet potato peel and (c) pomelo peel.

the carbonate ion band at 1550 cm^{-1} can be ascribed to A-type carbonate substitution on hydroxide ion sites [31]. In this experiment, the carbon peaks observed for the specimens closely matched those of A- and B-type carbonates.

The presence of carbonate is a form of lattice defect in the HA, which could contribute to its low crystallinity, supporting the XRD data. The more the powder is carbonated, the more the diffraction peaks broaden. These results show that AB mixed type carbonated apatites could be obtained from hydrothermal reaction processes that involved dissolution-precipitation phenomena. It should be mentioned that most biological apatites contain both A- and B-type carbonate ions in their lattices [31]. It can thereby be concluded that the prepared HA is chemically and structurally analogous to biological apatite. The apatite in natural bone contains significant amounts of carbonate ions, from about 4 to 6 wt % [32]. In general, low carbonate content can improve the bioactivity of HA [33].

3.3. Morphology and characterization

Figs. 3 and 4 represent the SEM micrographs of HA nanopowders prepared in the presence of three different biomolecular templates through hydrothermal reactions at 150 °C for 24 and 72 h, respectively. According to classical nucleation theory, heterogeneous nucleation always takes place earlier than homogeneous nucleation in a supersaturated solution, due to the lower free energies of nuclei on the surfaces of foreign bodies [34]. In the present study, biomolecules in the solution provide nucleation sites for the HA nuclei. The morphologies of synthetic HA crystals vary depending on the hydrothermal reaction times. After hydrothermal reaction at 150 °C for 24 h, aggregated particles with tiny needle-like or rod-like nanostructures were observed.

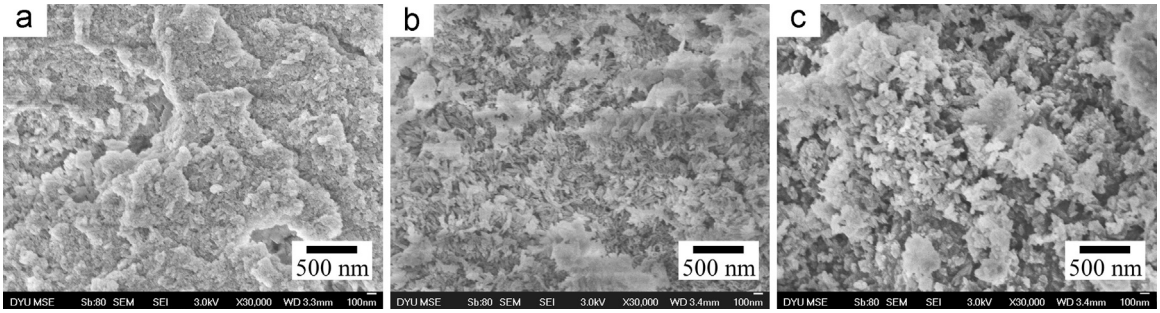

Fig. 3. SEM images of hydroxyapatite synthesized using three kinds of biomolecular templates in waste by hydrothermal treatment at 150 °C for 24 h. (a) Grape peel, (b) sweet potato peel and (c) pomelo peel.

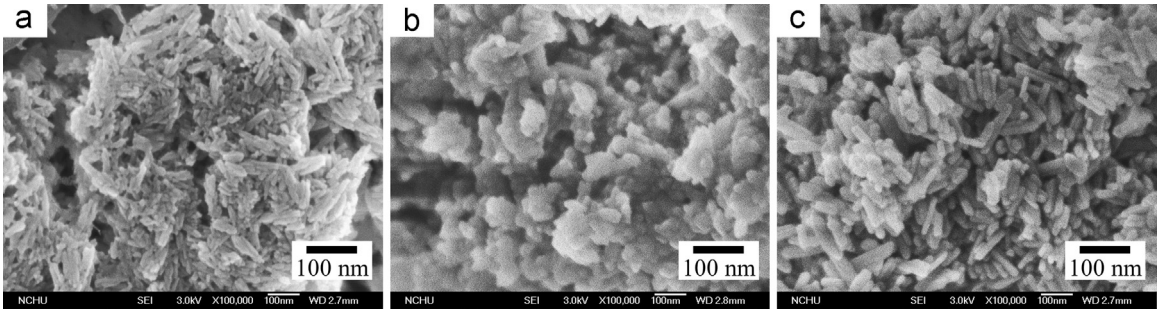

Fig. 4. SEM images of hydroxyapatite synthesized using three kinds of biomolecular templates in waste by hydrothermal treatment at 150 °C for 72 h. (a) Grape peel, (b) sweet potato peel and (c) pomelo peel.

Because nanoparticles have tiny volumes, their surface-to-volume ratios are much larger than those of larger particles. These high surface areas are accompanied by van der Waals interactions which result in a strong tendency to agglomerate [35]. As observed in SEM images, the presence of biomolecules influences the sizes and shapes of the products. The HA that was synthesized in the presence of grape peel extract exhibited more aggregation.

With a reaction time of 72 h, the needle-like nanostructures transformed into rod-like nanostructures and the aspect ratio decreased, as shown in Fig. 4. This phenomenon may be due to increased carbonate content. It is worth noting that the HA obtained from pomelo peel extract exhibited good aspect ratios with physical shapes similar to those of the crystalline hydroapatite structures of natural bone [36]. The limonene content in pomelo peel extract seems to have played a good role in controlling the shapes and sizes of the synthesized HA nanoparticles [37]. The HA formed using grape peel extract was an assembly of uniform rod-like nanoparticles. A close look shows that these agglomerates are made up of clusters of rods, each with a length less than 100 nm. The beta-carotene and other vitamins present in the grape peel extract are also seen to play an important role in controlling the sizes and shapes of HA nanoparticles [38]. The HA samples synthesized using sweet potato peel extract showed irregular aggregates of nanoparticles that resembled rice. The sizes and shapes of nanoparticles obtained from biogenic hydroxyapatite can preserve important characteristics such as good bioactivity and structural flexibility [39,40]. However the heating conditions should be controlled, since recrystallization can lead to growth of crystallite to slightly higher values than those reported for bones to be around 5–20 nm width by 60 nm length [41] and change the original tissue architecture.

The crystallite sizes of the synthesized HA nanopowders were calculated by Scherrer's formula as follows [42]:

$$Xs = 0.9\lambda/FWHM\cos\theta$$

where Xs is the average crystallite size (nm); λ is the wavelength of X-ray radiation (1.5406 Å); FWHM is the full width at half maximum for the diffraction peak under consideration (rad); and θ (degree) is the diffraction angle. The diffraction peak at $2\theta = 26.04^\circ$ was chosen for calculation of the crystallite size since it was isolated and sharper than the others.

The crystallite sizes of the HA nanoparticles obtained by the presence of grape, sweet potato, and pomelo peel extracts after 72 h were 32, 49, and 12 nm, respectively. The literature reports that bone crystals can be 30–50 nm in length, 15–30 nm in width, and 2–10 nm in thickness [32]. The nanostructure of bone-substituting materials is closely related to the good bioactivity and osteoconductivity. Synthetic HA composed of nanosized crystals can lead to an increase of osteoblast functions [43].

The results of measurements of elemental composition by an EDS method are presented in Fig. 5. The EDS spectra show sharp calcium and phosphorus peaks in the examined areas of the HA nanoparticles made from grape, sweet potato and pomelo peel extracts after 72 h. Furthermore, the EDS analysis revealed that the Ca/P molar ratios were between 1.57 and 1.77. The calculated Ca/P ratio is appreciable and fits quite

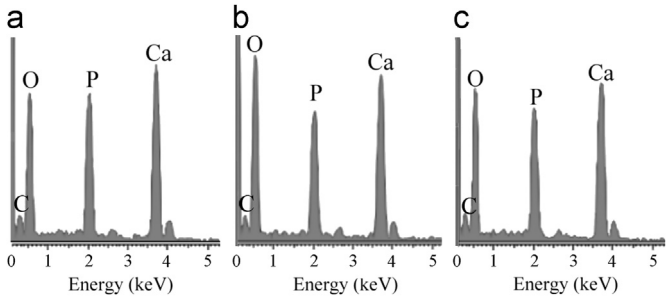

Fig. 5. EDS analyses for hydroxyapatite synthesized using three kinds of biomolecular templates in waste by hydrothermal treatment at 150 °C for 72 h. (a) Grape peel, (b) sweet potato peel and (c) pomelo peel.

well with that of biological apatite, which ranges from 1.50 to 1.85 [31]. It is worth pointing out that the Ca/P ratio of biological apatite mainly depends on the species and the age factor.

Not only are bone crystallites extremely small, they are often described as "poorly crystalline" because they show broad X-ray diffraction peaks (relative to stoichiometric HA), which are thought to arise from the incorporation of impurities, such as carbonate, sodium, and magnesium ions (4–6% carbonate; 0.9% Na; 0.5% Mg) [32], and from the nonstoichiometry of the biogenic mineral. The measurements of elemental composition by the ICP-AES method showed the presence of Ca (37.2 wt%), P (17.0 wt%), Na (0.410 wt%), Mg (0.390 wt%) and Sr (0.289 wt %) in the synthesized HA using pomelo peel extract after 72 h. Biological apatites have attracted particular interest because of the substitutions at the Ca^{2+}, PO_4^{3-}, and OH^- sites. The presence of several trace elements does not alter the basic crystallographic characteristics of HA, but can improve the overall biological performance of the implant material [44–47]. Ionic substitutions play an important role in bone formation. For example, strontium (Sr) could improve bone strength and provide benefits in the treatment of osteoporosis [48]. Sr-containing HA ceramics have exhibited mechanical properties better than those of pure HA, and have been shown to enhance the proliferation and differentiation of osteoblast cells in vitro [49]. Additionally, Na and Mg are known to be important trace elements in bones and teeth, and to play an important role in bone metabolism. Na and Mg depletion can cause bone fragility and bone loss [50,51]. Also, Mg plays a crucial role in cell proliferation and function [51].

4. Conclusions

The present study suggests recycled chicken eggshells can improve the ecosphere by reducing the need for waste management; furthermore, these eggshells can provide useful raw materials for nanomaterials. This research describes how nano-sized HA powders were successfully prepared using biomolecular templates from waste materials (grape, sweet potato, and pomelo peel extracts) after hydrothermal reactions at 150 °C. Our results indicate the following important points:

(1) The HA nanopowders that were synthesized from three different biomolecular templates have similar XRD patterns and no other crystalline phase can be observed besides HA. The broad peaks in the XRD patterns point out the small size and low crystallinity of the HA, which is similar to naturally occurring bone apatite.
(2) All HA synthesized using three different biomolecular templates have similar FT-IR spectra. The carbon peaks observed for the specimens closely matched those of A- and B-type carbonate, which could contribute to the low crystallinity of the synthesized HA.
(3) After hydrothermal reactions at 150 °C for 24 h, aggregated particles with tiny needle-like or rod-like nanostructure were observed. Needle-like nanostructures transformed into rod-like nanostructures and the aspect ratio decreased after hydrothermal reactions for 72 h. The HA obtained using pomelo peel extract exhibited good aspect ratios with physical shapes similar to those of the crystalline hydroapatite structures of natural bone.
(4) The crystallite sizes of the HA nanoparticles obtained using grape, sweet potato, and pomelo peel extracts after hydrothermal reactions at 150 °C for 72 h were 32, 49, and 12 nm, respectively.
(5) ICP-AES evaluations showed the presence of Ca (37.2 wt%), P (17.0 wt%), Na (0.410 wt%), Mg (0.390 wt%) and Sr (0.289 wt%) in the HA synthesized from pomelo peel extract.

Acknowledgment

The authors acknowledge the partial financial support of Taichung Veterans General Hospital and Da-Yeh University (TCVGH-DYU1028304).

References

[1] G. Willmann, Medical grade hydroxyapatite: state of the art, British Ceramic Transactions 95 (1996) 212–216.
[2] S.M. Best, A.E. Porter, E.S. Thian, J. Huang, Bioceramics: past, present and for the future, Journal of the European Ceramic Society 28 (2008) 1319–1327.
[3] C. Balazsi, F. Weber, Z. Kover, E. Horrath, C. Nemth, Preparation of calcium–phosphate bioceramics from natural resources, Journal of the European Ceramic Society 27 (2007) 1601–1606.
[4] C.T. Laurencin, M.A. Attawia, L.Q. Lu, M.D. Borden, H.H. Lu, W. J. Gorum, J.R. Lieberman, Poly(lactide-co-glycolide)/hydroxyapatite delivery of BMP-2-producing cells: a regional gene therapy approach to bone regeneration, Biomaterials 22 (2001) 1271–1277.
[5] K.C.B. Yeong, J. Wang, S.C. Ng, Mechanochemical synthesis of nanocrystalline hydroxyapatite from CaO and $CaHPO_4$, Biomaterials 22 (2001) 2705–2712.
[6] A.P. Shpak, V.L. Karbovskii, A.G. Vakh, Electronic structure of isomorphically substituted strontium apatite, Journal of Electron Spectroscopy 585 (2004) 137–140.
[7] S. Kannan, A. Rebelo, J.M.F. Ferreira, Novel synthesis and structural characterization of fluorine and chlorine co-substituted hydroxyapatites, Journal of Inorganic Biochemistry 100 (2006) 1692–1697.
[8] E. Landi, G. Celotti, G. Logroscino, A. Tampieri, Carbonated hydroxyapatite as bone substitute, Journal of the European Ceramic Society 23 (2003) 2931–2937.

[9] S.J. Kalita, A. Bhardwaj, H.A. Bhatt, Nanocrystalline calcium phosphate ceramics in biomedical engineering, Materials Science and Engineering C 27 (2007) 441–449.
[10] T. Yuasa, Y. Miyamoto, K. Ishikawa, M. Takechi, Y. Momota, S. Tatehara, M. NagayamaM, Effects of apatite cements on proliferation and differentiation of human osteoblasts in vitro, Biomaterials 25 (2004) 1159–1166.
[11] L.S. Ozyegin, F.N. Oktar, G. Gollerc, E.S. Kayalic, T. Yazicic, Plasma-sprayed bovine hydroxyapatite coatings, Materials Letters 58 (2004) 2605–2609.
[12] M. Ozawa, S Suzuki, Microstructural development of natural hydroxyapatite originated from fish-bone waste through heat treatment, Journal of the American Ceramic Society 85 (2002) 1315–1317.
[13] S.C. Wu, H.C. Hsu, Y.N. Wu, W.F. Ho, Hydroxyapatite synthesized from oyster shell powders by ball milling and heat treatment, Materials Characterization 62 (2011) 1180–1187.
[14] D.M. Roy, S.K. Linnehan, Hydroxyapatite formed from coral skeletal carbonate by hydrothermal exchange, Nature 247 (1974) 220–222.
[15] M. Sivakumar, T.S.S. Kumar, K.L. Shantha, K.P. Rao, Development of hydroxyapatite derived from Indian coral, Biomaterials 17 (1996) 1709–1714.
[16] J. Hu, J.J. Russell, B. Ben-Nissan, R. Vago, Production and analysis of hydroxyapatite from Australian corals via hydrothermal process, Journal of Materials Science 20 (2001) 85–87.
[17] S.C. Wu, H.C. Hsu, S.K. Hsu, C.W. Hung, W.F. Ho, Calcium phosphate bioceramics synthesized from eggshell powders through a solid state reaction, Ceramic International (2013) http://dx.doi.org/10.1016/j.ceramint.2013.01.076.
[18] M.K. Herliansyah, M. Hamdi, A. Ide-Ektessabi, M.W. Wildan, J.A. Toque, The influence of sintering temperature on the properties of compacted bovine hydroxyapatite, Materials Science and Engineering C 29 (2009) 1674–1680.
[19] J.W. Park, S.R. Bae, J.Y. Suh, D.H. Lee, S.H. Kim, H. Kim, C.S. Lee, Evaluation of bone healing with eggshell-derived bone graft substitutes in rat calvaria: a pilot study, Journal of Biomedical Materials Research Part A 87 (2008) 203–214.
[20] A. Siddharthan, T.S. Sampath Kumar, S.K. Seshadri, Synthesis and characterization of nanocrystalline apatites from eggshells at different Ca/P ratios, Biomedical Materials 4 (2009) 045010–045019.
[21] E.M. Rivera, M. Araiza, W. Brostow, V.M. Castaño, J.R. Díaz-Estrada, R. Hernández, J.R. Rodríguez, Synthesis of hydroxyapatite from eggshells, Materials Letters 41 (1999) 128–134.
[22] C.M. Zhang, J. Yang, Z.W. Quan, P.P. Yang, C.X. Li, Z.Y. Hou, J. Lin, Hydroxyapatite nano- and microcrystals with multiform morphologies: controllable synthesis and luminescence properties, Crystal Growth and Design 9 (2009) 2725–2733.
[23] C. Negro, L. Tommasi, A. Miceli, Phenolic compounds and antioxidative activity from red grape marc extracts, Bioresource Technology 87 (2003) 431–444.
[24] A. Al-Weshahy, A. Venket Rao, Isolation and characterization of functional components from peel samples of six potatoes varieties growing in Ontario, Food Research International 42 (2009) 1062–1066.
[25] M. Senevirathne, Y.J. Jeon, J.H. Ha, S.H. Kim, Effective drying of citrus by-product by high speed drying: A novel drying technique and their antioxidant activity, Journal of Food Engineering 92 (2009) 157–163.
[26] N.T. Minh Tu, L.X. Thanh, A. Une, H. Ukeda, M. Sawamura, Volatile constituents of Vietnamese pummelo, orange, tangerine and lime peel oils, Flavour and Fragrance Journal 17 (2002) 169–174.
[27] S. Nayar, A. Guha, Waste utilization for the controlled synthesis of nanosized hydroxyapatite, Materials. Science and Engineering C 29 (2009) 1326–1329.
[28] H.M. Kim, Y. Kim, S.J. Park, C. Rey, H.M. Lee, M.J. Gimcher, J.S. Ko, Thin film of low-crystalline calcium phosphate apatite formed at low temperature, Biomaterials 21 (2000) 1129–1134.
[29] K. Prabakaran, S. Rajeswari, Spectroscopic investigations on the synthesis of nano-hydroxyapatite from calcined eggshell by hydrothermal method using cationic surfactant as template, Spectrochimica Acta A 74 (2009) 1127–1134.
[30] A. Stoch, W. Jastrzębski, A. Brożek, J. Stoch, J. Szaraniec, B. Trybalska, G. Kmita, FTIR absorption–reflection study of biomimetic growth of phosphates on titanium implants, Journal of Molecular Structure 555 (2000) 375–382.
[31] R. Murugan, S. Ramakrishna, Production of ultra-fine bioresorbable carbonated hydroxyapatite, Acta Biomaterialia 2 (2006) 201–206.
[32] M.J. Olszta, X. Cheng, S.S. Jee, R. Kumar, Y.Y. Kim, M.J. Kaufman, E.P. Douglas, L.B. Coger, Bone structure and formation: a new perspective, Materials Science and Engineering R 58 (2007) 77–116.
[33] S.A. Redey, S. Razzouk, C. Rey, D. Bernache-Assollant, G. Leroy, M. Nardin, G. Cournot, Osteoclast adhesion and activity on synthetic hydroxyapatite, carbonated hydroxyapatite and natural calcium carbonate: Relationship to surface energies, Journal of Biomedical Materials Research 45 (1999) 140–147.
[34] P.X. Zhu, Y. Masuda, K. Koumoto, The effect of surface charge on hydroxyapatite nucleation, Biomaterials 25 (2004) 3915–3921.
[35] R. Ebrahimi-Kahrizsangi, B. Nasiri-Tabrizi, A. Chami, Synthesis and characterization of fluorapatite–titania (FAp–TiO_2) nanocomposite via mechanochemical process, Solid State Sciences 12 (2010) 1645–1651.
[36] X.M. Li, Q.L. Feng, F.H. Cui, In vitro degradation of porous nano-hydroxyapatite/collagen/PLLA scaffold reinforced by chitin fibres, Materials Science and Engineering C 26 (2006) 716–720.
[37] M.H. Boelens, R. Jimenez, The chemical composition of the peel oil from unripe and ripe fruits of bitter orange, *Citrus aurantium* L. ssp. amara engl, Flavour and Fragrance Journal 4 (1989) 139–142.
[38] J. Augustin, R.B. Toma, R.H. True, L.R. Shaw, C. Teitzel, S.R. Johnson, P. Orr, Composition of raw and cooked potato peel and flesh: proximate and vitamin composition, Journal of Food Science 44 (1979) 805–806.
[39] J. Huang, Y.W. Lin, X.W. Fu, S.M. Best, R.A. Brooks, N. Rushton, W. Bonfield, Development of nano-sized hydroxyapatite reinforced composites for tissue engineering scaffolds, Journal of Materials Science: Materials in Medicine 18 (2007) 2151–2157.
[40] J. Chevalier, L. Gremillard, Ceramics for medical applications: a picture for the next 20 years, Journal of European Ceramic Society 29 (2009) 1245–1255.
[41] W. Paul, C.P. Sharma, Nanoceramic matrices: biomedical applications, American Journal of Biochemistry and Biotechnology 2 (2006) 41–48.
[42] M.H. Fathia, A. Hanifia, V. Mortazavi, Preparation and bioactivity evaluation of bone-like hydroxyapatite nanopowder, Journal of Materials Processing Technology 202 (2008) 536–542.
[43] G. Balasundaram, M. Sato, T.J. Webster, Using hydroxyapatite nanoparticles and decreased crystallinity to promote osteoblast adhesion similar to functionalizing with RGD, Biomaterials 27 (2006) 2798–2805.
[44] S. Cazalbou, C. Combes, D. Eichert, C. Rey, Adaptative physicochemistry of bio-related calcium phosphates, Journal of Materials Chemistry 14 (2004) 2148–2153.
[45] W. Suchanek, K. Byrappa, P. Shuk, R.E. Riman, V.F. Janas, K. S. TenHuisen, Preparation of magnesium-substituted hydroxyapatite powders by the mechanochemical–hydrothermal method, Biomaterials 25 (2004) 4647–4657.
[46] I.R. Gibson, W. Bonfield, Preparation and characterization of magnesium/carbonate co-substituted hydroxyapatites, Journal of Materials Science: Materials in Medicine 13 (2002) 685–693.
[47] S. Kannan, J.M. Ventura, J.M.F. Ferreira, In situ formation and characterization of flourine-substituted biphasic calcium phosphate ceramics of varied F-HAP/β-TCP ratios, Chemistry of Materials 17 (2005) 3065–3068.
[48] S.G. Dahl, P. Allain, P.J. Marie, Y. Mauras, G. Boivin, P. Ammann, Y. Tsouderos, P.D. Delmas, C. Christiansen, Incorporation and distribution of strontium in bone, Bone 28 (2001) 446–453.
[49] E. Landi, A. Tampieri, G. Celotti, S. Sprio, M. Sandri, G. Logroscino, Sr-substituted hydroxyapatites for osteoporotic bone replacement, Acta Biomaterialia 3 (2007) 961–969.
[50] E. Boanini, M. Gazzano, A. Bigi, Ionic substitutions in calcium phosphates synthesized at low temperature, Acta Biomaterialia 6 (2010) 1882–1894.
[51] R.K. Rude, H.E. Gruber, Magnesium deficiency and osteoporosis: animal and human observations, Journal of Nutritional Biochemistry 15 (2004) 710–716.